

Electronic Supplementary Information (ESI) for
Enhanced Cr(VI) Immobilization on Goethite Derived from
Extremely Acidic Environment

*Xiaobing Wang, Na Chen, and Lizhi Zhang*¹*

Key Laboratory of Pesticide & Chemical Biology of Ministry of Education, Institute of
Environmental & Applied Chemistry, Central China Normal University, Wuhan 430079, P. R. China

11 pages, 3 texts, 9 figures, 3 tables

* To whom correspondence should be addressed. E-mail: zhanglz@mail.ccnu.edu.cn(L. Zhang).
Phone/Fax: +86-27-6786 7535.

CONTENTS

Text S1. Influence of the synthesis temperature of GB on Cr(VI) immobilization	S3
Text S2. DFT theoretical calculation	S4
Text S3. Cr(III) immobilization on GA and GB	S5
Figure S1. XRD patterns of different samples	S6
Figure S2. SEM images of GA and GB	S6
Figure S3. Schematic illustrations of GA and GB	S7
Figure S4. Langmuir and Freundlich models for the adsorption of Cr(VI) on goethite	S7
Figure S5. Characterization of GB-80 and Cr(VI) immobilization behavior	S8
Figure S6. Zeta potentials of GA and GB	S8
Figure S7. Slabs used to represent the goethite {110} and {021} surface	S9
Figure S8. Raw Cr K-edge X-ray absorption spectra for Cr(VI) treated goethite	S9
Figure S9. Cr(III) immobilization behavior on goethite	S9
Table S1. Kinetics and equilibrium parameters of Cr(VI) adsorption on goethite	S10
Table S2. Parameters obtained from Langmuir and Freundlich isotherms	S10
Table S3. Kinetic parameters for adsorption of Cr(III) on goethite	S10
References	S11

Text S1. Influence of synthesis temperature on Cr(VI) immobilization. As reported by Müller et al., when the hydrolysis of Fe(III) occurred in the acidic condition, the high temperature was unfavourable for the formation of goethite, so that Fe₂O₃ would be produced in the forced hydrolysis process.¹ According to the synthetic method reported by Kakuta et al., the forced hydrolysis temperature of Fe(III) was set as 80 °C, which was suitable for the production of pure goethite in this study.² To evaluate the influence of temperature on the formation of GB, we also synthesized the iron mineral in the alkaline condition under 80 °C (called as GB-80). XRD patterns revealed that the crystallinity of GB formed at 80 °C was slightly lower than that of GB synthesized at 100 °C (called as GB-100) in this study, but their morphologies were the same (Figure S5a-c). Subsequently, we compared the BET specific surface areas of GB-80 and GB-100, and found that the BET specific surface area (51 m²/g) of GB-80 was slightly higher than that (46 m²/g) of GB-100. Furthermore, we carefully checked the Cr(VI) adsorption performances of GA, GB-80, and GB-100 (Figure S5d-e). After the normalization of the specific surface area, the Cr(VI) immobilization capacity of GB-80 was 0.094 mg·m⁻², lower than that (0.124 mg·m⁻²) of GA. On the basis of the pseudo-second-order non-linear kinetic model, the apparent Cr(VI) removal rate constant (6.39 m²·mg⁻¹·min⁻¹) of GB-80 was also lower than that (15.68 m²·mg⁻¹·min⁻¹) of GA. Therefore, even though the synthesis temperature of GB was lowered to 80 °C, GA could still exhibit faster adsorption rate and larger immobilization capacity than GB.

Text S2. DFT theoretical calculation. The calculations were performed by density functional theory (DFT) as implemented in the software Gaussian 09.³ The goethite cluster was established on the basis of its lattice structure. The hybrid B3LYP density functional with the Lanl2dz basis set was used for geometry optimization and frequency calculations.⁴⁻⁶ The polarizable continuum alvation model which derived from the self-consistent reaction field (SCRF) theory was used to calculate the long-range solvent polarization effects of clusters in water.⁷

Text S3. Cr(III) immobilization on GA and GB. Cr(III) was a dominating species in the extremely acidic environment such as the acid mine drainage.⁸ Hence, we investigated the adsorption performance of Cr(III) on the two goethite minerals. It was found that Cr(III) could not be efficiently immobilized by both of the two minerals under the extremely acidic environment with a pH value of 1.8 (Figure S9a). The poor adsorption ability might be attributed to the much higher positive zeta potential of goethite under the extremely acidic environment. Furthermore, we investigated the Cr(III) immobilization under a pH value of 5.7 which was selected for the Cr(VI) adsorption experiment in our studies. After the normalization of the specific surface area, the apparent Cr(III) removal rate constant from the pseudo-second-order non-linear kinetic model was $8.92 \text{ g} \cdot \text{mg}^{-1} \cdot \text{min}^{-1}$ for GA, which was 133 times that of GB ($0.067 \text{ g} \cdot \text{mg}^{-1} \cdot \text{min}^{-1}$), indicating Cr(III) was more efficiently adsorbed on GA. However, the Cr(III) immobilization equilibrium capacity of GA was $0.0165 \text{ mg} \cdot \text{m}^{-2}$, only one-third of GB's capacity ($0.050 \text{ mg} \cdot \text{m}^{-2}$) (Figure S9b). The above results revealed that the Cr(III) could be adsorbed faster on the GA surface, but with lower equilibrium capacity. The parameters obtained from the pseudo-second-order non-linear kinetic model were presented in Table S3.

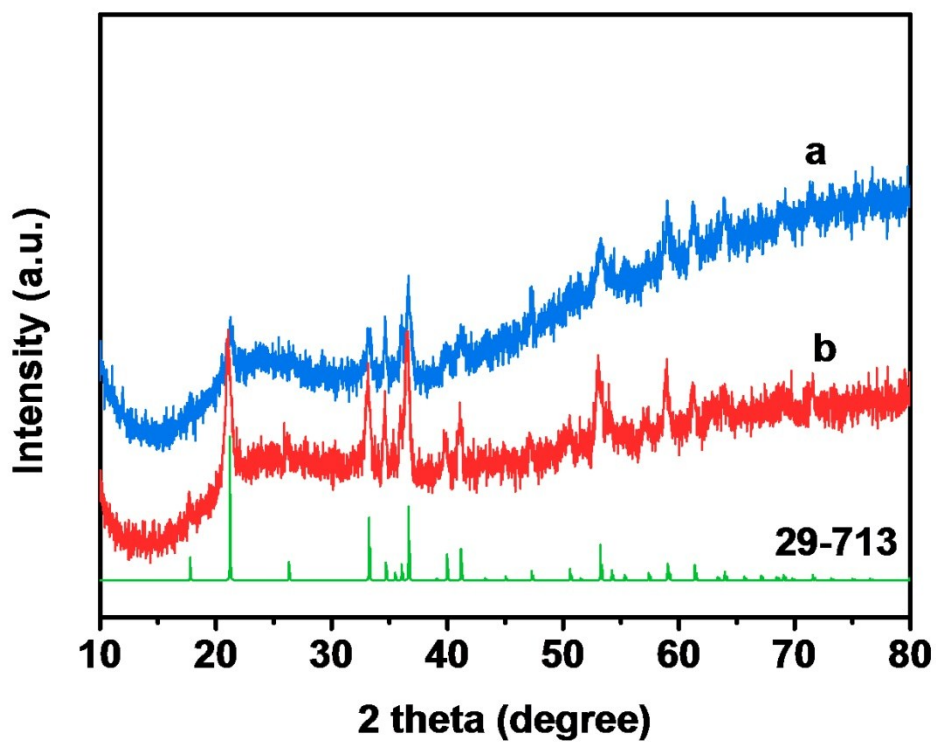


Figure S1. XRD patterns of the two samples: (a) GA and (b) GB.

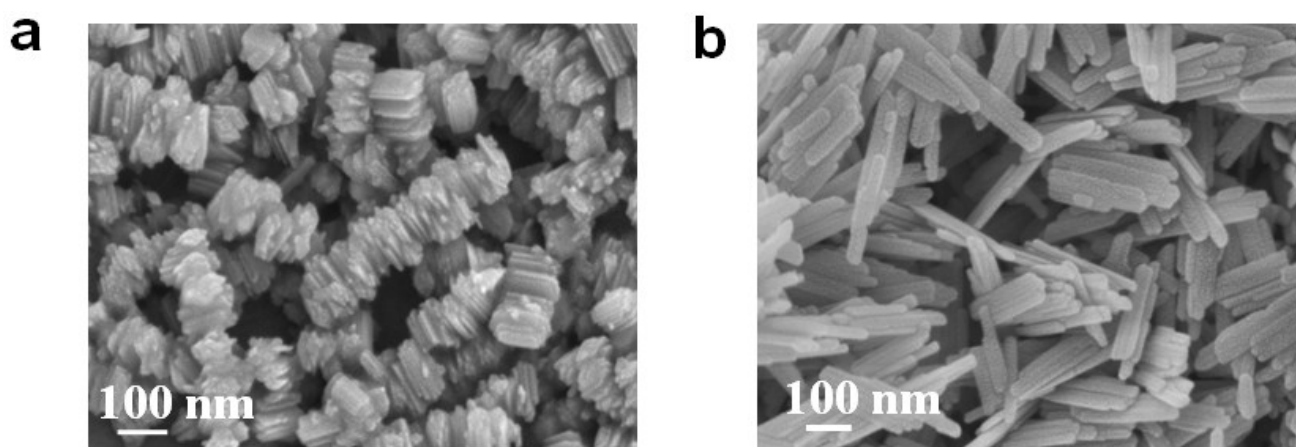


Figure S2. SEM images of the prepared goethite: (a) GA and (b) GB.

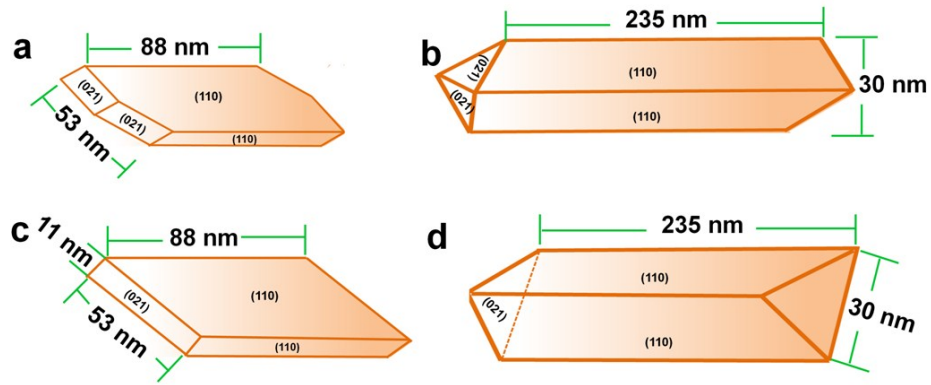


Figure S3. Schematic illustrations of the different facets on goethite: (a) GA and (b) GB. The simplified models for the calculation of $\{021\}/\{110\}$ facet proportion of goethite: (c) GA and (d) GB.

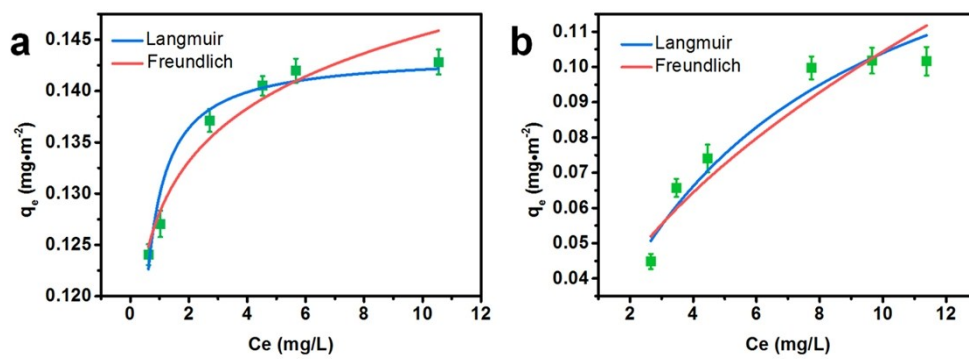


Figure S4. (a) Langmuir plot and Freundlich plot for the adsorption of Cr(VI) ions on GA. (b) Langmuir plot and Freundlich plot for the adsorption of Cr(VI) ions on GB. The initial Cr(VI) concentrations were from 4 to 14 $\text{mg}\cdot\text{L}^{-1}$; The dosage of goethite were 0.5 $\text{g}\cdot\text{L}^{-1}$; The initial pH values of the systems were 5.7.

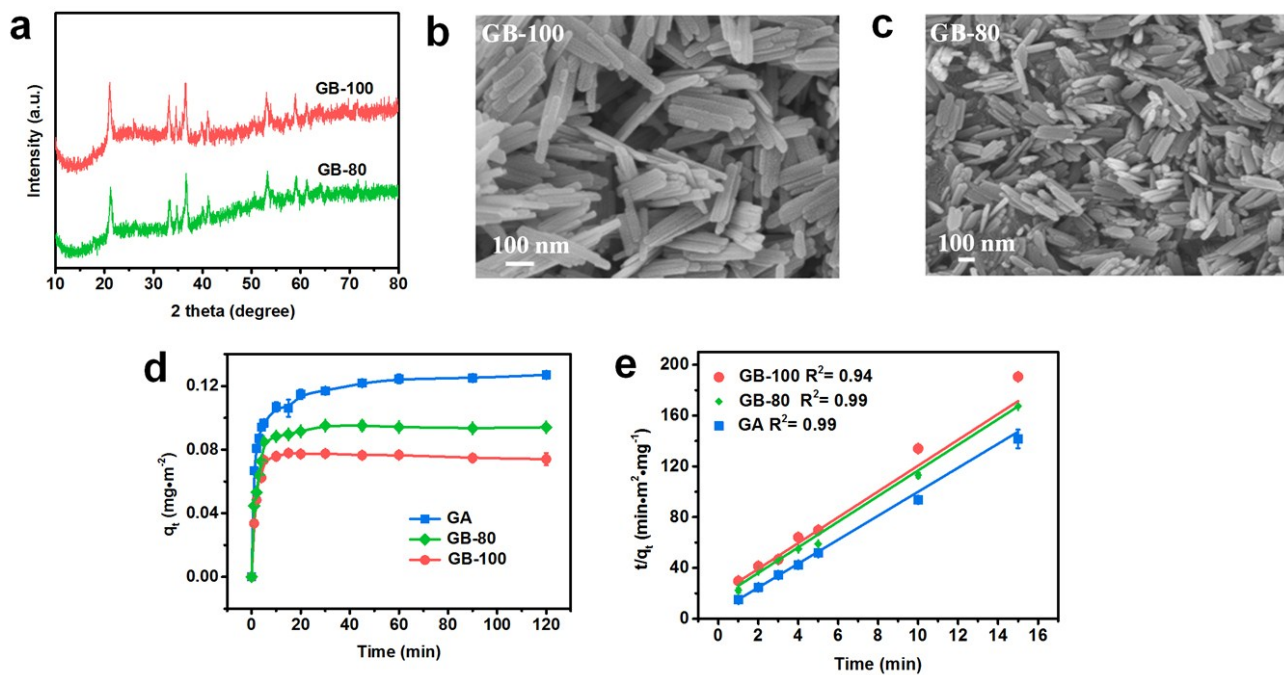


Figure S5. (a) XRD and (b) SEM of GB synthesized under 100 °C. (c) SEM of GB synthesized under 80 °C. (d) Time profile of Cr(VI) ions removal with goethite. (e) The corresponding removal kinetics curves of Cr(VI) ions on goethite. The initial concentrations of Cr(VI) and goethite were 5 mg·L⁻¹ and 0.5 g·L⁻¹.

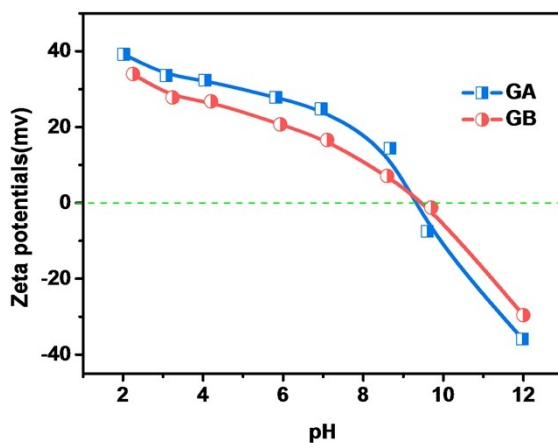


Figure S6. Zeta potentials of GA and GB.

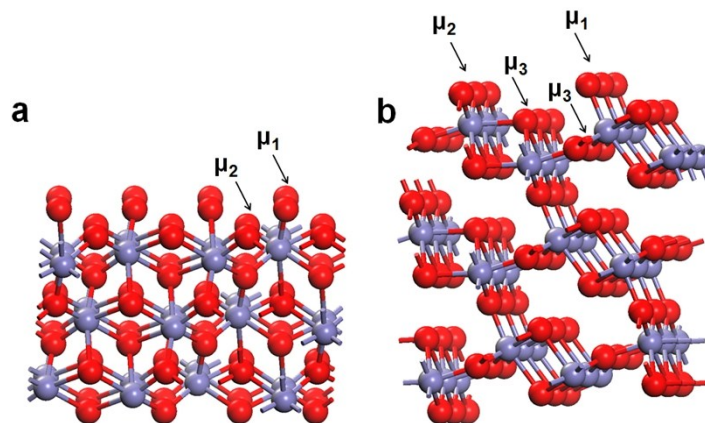


Figure S7. Slabs used to represent the goethite surface: (a) {110} plane and (b) {021} plane.

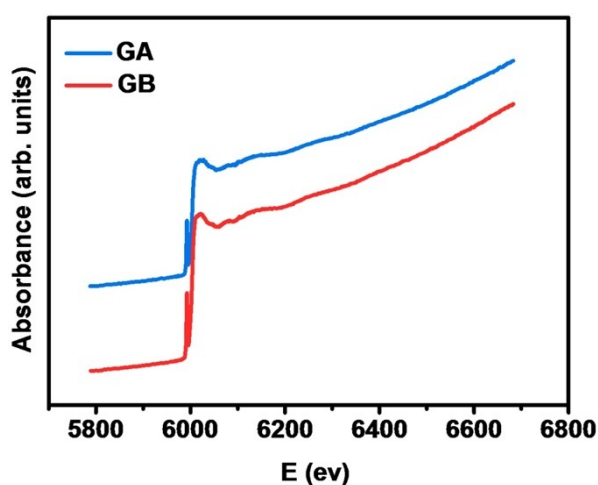


Figure S8. Raw Cr K-edge X-ray absorption spectra for Cr(VI) treated goethite.

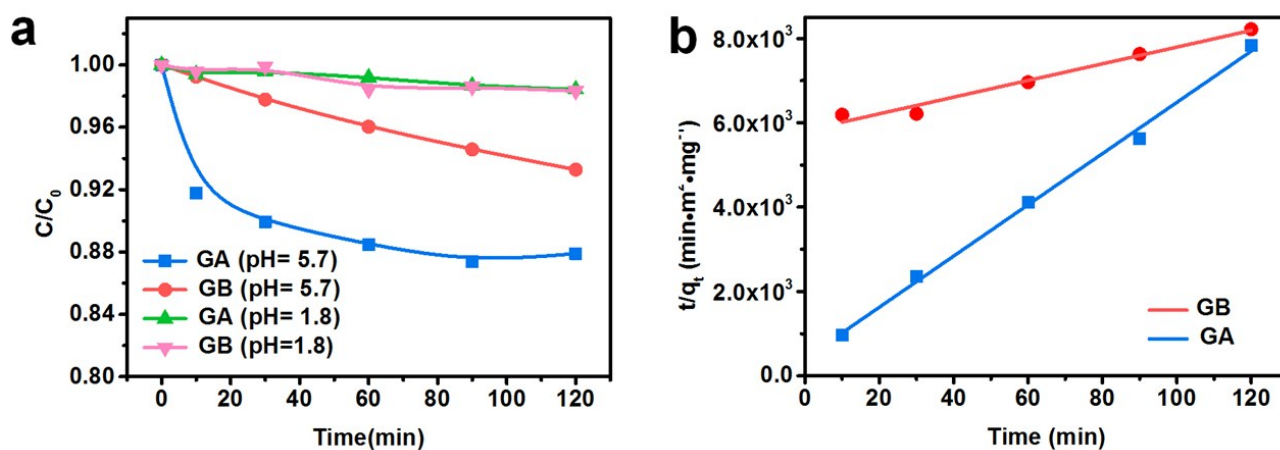


Figure S9. (a) Time profile of Cr(III) ions removal with goethite. (b) The corresponding removal kinetics curves of Cr(III) ions on goethite. The initial concentrations of Cr(III) and goethite were $5 \text{ mg}\cdot\text{L}^{-1}$ and $0.5 \text{ g}\cdot\text{L}^{-1}$.

Table S1. Kinetics and equilibrium parameters of Cr(VI) adsorption on goethite

entry	SSA ^a (m ² ·g ⁻¹)	q_e (mg·m ⁻²)	k_2 (m ² ·mg ⁻¹ ·min ⁻¹)	R ²	q_m (mg·m ⁻²)
GA	79	0.124	15.68	0.99	0.143
GB	46	0.075	5.44	0.94	0.101

Table S2. Parameters obtained from the Langmuir and Freundlich isotherms for the adsorption of Cr(VI) on goethite

Model	Parameters	GA	GB
Langmuir	q_m /(mg·m ⁻²)	0.144	0.127
	K_L /(L·mg ⁻¹)	9.44	0.163
	R ²	0.96	0.93
Freundlich	1/n	0.055	0.527
	K_F /(mg/g)/(mg/L) ^{1/n}	0.128	0.031
	R ²	0.93	0.88

Table S3. Kinetic parameters for adsorption of Cr(III) on goethite

Parameters	GA	GB
K (g/mg·min)	8.92	0.067
q_e /(mg·m ⁻²)	0.017	0.030
R ²	0.99	0.97

References

1. M. Müller, J. C. Villalba, F. Q. Mariani, M. Dalpasquale, M. Z. Lemos, M. F. G. Huila and F. J. Anaissi, Synthesis and characterization of iron oxide pigments through the method of the forced hydrolysis of inorganic salts. *Dyes and Pigments*, 2015, **120**, 271-278.
2. S. Kakuta, T. Numata and T. Okayama, Shape effects of goethite particles on their photocatalytic activity in the decomposition of acetaldehyde. *Catal. Sci. Technol.*, 2014, **4**, 164-169.
3. M. J. Frisch, G. W. Trucks, H. B. Schlegel, G. E. Scuseria, M. A. Robb, et al., *Gaussian 09, Revision A. 1*; Gaussian, Inc.: Wallingford, CT, 2009.
4. A. D. Becke, Density-functional thermochemistry. III. The role of exact exchange. *J. Chem. Phys.*, 1993, **98**, 5648-5652.
5. C. E. Check, T. O. Faust, J. M. Bailey, B. J. Wright, T. M. Gilbert and L. S. Sunderlin, Addition of polarization and diffuse functions to the LANL2DZ Basis set for P-block elements. *J. Phys. Chem. A*, 2001, **105**, 8111-8116.
6. S. Bell and T. J. Dines, An ab initio study of the structures and vibrational spectra of chromium oxo-anions and oxyhalides. *J. Phys. Chem. A*, 2000, **104**, 11403-11413.
7. B. Mennucci, E. Cancès and J. Tomasi, Evaluation of solvent effects in isotropic and anisotropic dielectrics and in ionic solutions with a unified integral equation method: Theoretical bases, computational implementation, and numerical applications. *J. Phys. Chem. B*, 1997, **101**, 10506-10517.
8. G. Singh and N. S. Rawat, Removal of trace elements from acid mine drainage. *Int. J. Mine water*, 1985, **4**, 17-23.